Frequency domain analysis of surface errors based on imaging performance

Shan Wu, Jinshi Wang #, and Fengzhou Fang #

State Key Laboratory of Precision Measurement Technology & Instruments, Laboratory of MicroNano Manufacturing Technology—MNMT, Tianjin University, 300072, China
Corresponding Author / Email: jswang@tju.edu.cn, fzfang@tju.edu.cn

KEYWORDS: surface errors, frequency category, point spread function

Surface errors introduced during the manufacturing process can be categorized into low, middle, and high spatial frequency regions of the power spectral density function. These regions have distinct effects on image quality, particularly on the diffraction-limited point spread function. Generally, low spatial frequency errors produce conventional aberrations, middle spatial frequency errors result in small-angle scatter and high spatial frequency errors cause wide-angle scatter. However, the cutoff frequencies separating these regions are not clearly defined and largely depend on design and manufacturing experience. This paper presents a surface error model for a Cooke triplet system that utilizes sinusoids to represent structural errors in ultra-precision diamond turning. Additionally, the relationships between cutoff frequencies and diffraction PSFs are systematically investigated, with particular emphasis on their correlation to the field of view, surface position, and working wavelength.

1. Introduction

Surface errors generated during the manufacturing process significantly impact image performance [1, 2]. These errors can be categorized into low, middle, and high spatial frequency regions based on the power spectral density function (PSD) of the surface, with each region affecting the resulting image quality differently. Generally, low spatial frequency errors transfer energy from the focused spot center to the initial few diffraction rings, typically analyzed using ray tracing based on fitted surfaces derived from measurement data. Middle spatial frequency irregularities cause small-angle scatter, substantially reducing resolution, while high spatial frequency surface roughness scatters energy away from the spot center, resulting in a broad scattering halo [3, 4]. Nevertheless, there are various definitions of the cutoff frequencies between the three regions in the literature.

Aikens et al. [5] have defined the middle-frequency range as falling between low-frequency errors characterized by a 37-term Zernike polynomial expansion and low-frequency errors, where the Fresnel lengths of the patterns are less than 1/10 of the optical path distance from a given surface to the image plane. Tamkin et al. [6] proposed a cutoff frequency of 1/20 of Nyquist frequency to differentiate middle spatial frequencies from surface roughness. For visible wavelengths, the middle spatial frequency region typically spans from a few millimeters to 0.1 millimeters [7]. However, the definite establishment of the cutoff frequencies may be more complex, as they are influenced by factors such as the fields of view (FOV), surface positions, and working wavelengths [8].

In this paper, a surface error model based on sinusoids for a Cooke triplet system is established to analyze the cutoff frequencies of the structural errors in ultra-precision diamond turning. The relationships between these errors and diffraction PSFs are systematically studied, which are related to FOVs, surface positions, and working wavelengths.

2. Error model and numerical analysis

2.1 Design and error model of the Cooke triplet system

The designed optical system exhibits diffraction-limited performance, as illustrated in Fig. 1(a). The aperture stop is located on surface S3, and the working wavelength ranges from 486 nm to 656 nm, with 546 nm being the dominant wavelength. The full field of view is 40°. Surfaces S1, S3, and S5 are aspheric, whereas surfaces S2, S4, and S6 are conic. Detailed design parameters are presented in Table 1.

The layout (Fig. 1(a)) illustrates the design of the Cooke triplet system, featuring a beam footprint on S1, S3, and S5 for 0°、14°and 20° FOVs. When a surface with machining errors is near the stop (S3), the bundles for the three FOVs fully illuminate the surface. In contrast, when the optical surfaces are distant from the stop (S1 and S5), the beam footprint on these surfaces occupies only a fraction of the part's diameter, indicating that only a portion of the error on the surface will affect imaging quality. The spot diagram for the system (Fig. 1(b))

shows root mean square (RMS) spot radii ranging from a maximum of 0.773 μm to a minimum of 1.316 μm, which are smaller than the Airy disk radius of 3.379 μm for the dominant wavelength. The modulation transfer function (MTF) curves are presented in Fig. 1(c), with the solid line representing the meridian direction and the dotted line representing the sagittal direction. Both the spot diagram and the MTF curves confirm that the system has achieved diffraction-limited performance.

Table 1 The designed parameters of the Cooke triplet system

Surface	1	2	3	4	5	6
Radius	20.883	-6.712	8.687	3.623	7.986	-17.301
Conic Constant	17.209	-6.214	55.563	-1.701	2.145	-217.479
4^{th} coefficient	-8.124E-04	0.000	-8.875E-03	0.000	4.510E-04	0.000
6^{th} coefficient	2.297E-06	0.000	-5.895E-03	0.000	-1.863E-04	0.000
8^{th} coefficient	3.869E-07	0.000	2.129E-03	0.000	1.019E-05	0.000
10^{th} coefficient	-3.895E-08	0.000	-4.791E-03	0.000	-3.250E-07	0.000
Thickness	1.500	2.500	0.800	3.500	1.500	6.319

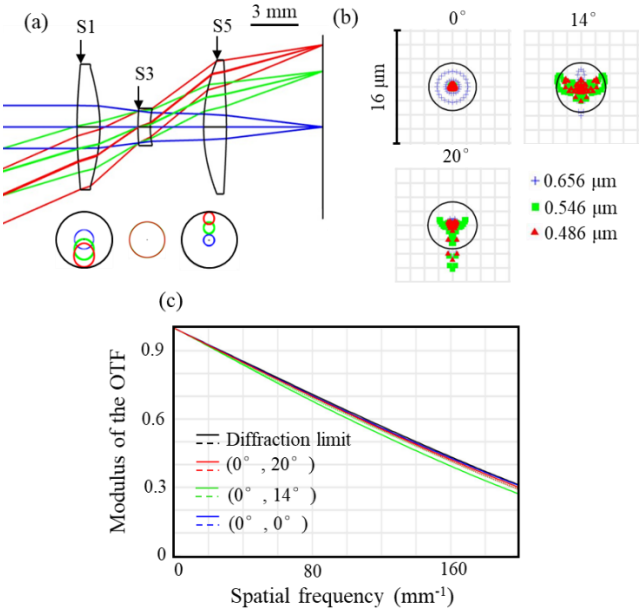

Fig.1 (a) The layout, (b) the spot diagram, and (c) the MTF curves of the designed Cooke triplet system.

To analyze the impact of machining errors on imaging performance, a surface error model utilizing sinusoids is established as expressed in Eq. (1):

$$z = \frac{cr^2}{1+\sqrt{1-(1+k)c^2r^2}} + \sum_{i=2}^{5}\alpha_i r^{2i} + A\sin(2\pi\omega_0 r) \quad (1)$$

where c is the radius of curvature, k represents the conic constant, α_i designates the aspheric coefficient, A is the amplitude of the surface error, and ω_0 denotes the frequency of the surface error. The first two terms in the equation represent ideal surfaces without errors. Diffraction calculations are conducted using CODE V Beam Synthesis Propagation to generate the image point spread functions (PSFs). The ideal PSFs at the dominant wavelength for 0° 、14° and 20° FOVs are illustrated in Fig. 2, demonstrating that there is no significant diffraction effect and that most of the energy is concentrated at the center of the focused spot.

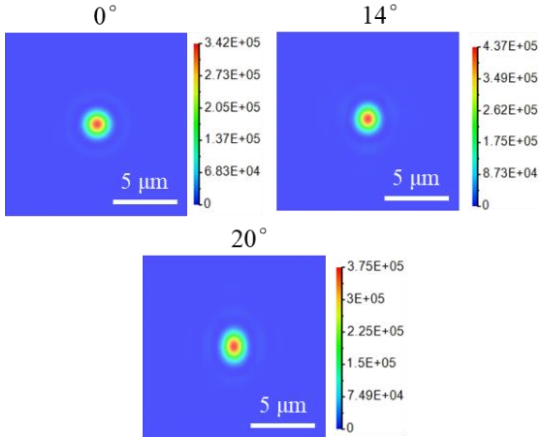

Fig. 2 The ideal PSFs at the dominant wavelength for 0° 、14° and 20° FOVs on the image plane, respectively.

2.2 Effects of machining errors in different spatial frequencies

Surface errors can be categorized into low, middle, and high spatial frequency regions of the surface PSD due to their varying effects on the resulting image quality. Additionally, this categorization is influenced by factors such as the FOVs, surface positions, and working wavelengths. Even when surfaces are fabricated using the same process and exhibit similar surface errors, their impact on image performance can differ significantly.

When the surfaces are located far from the stop (S3), as depicted by S1 in Fig. 1(a), the beam footprint occupies only a fraction of the part diameter. Consequently, the effects of surface errors on imaging performance are dependent on the FOVs. Figure 3 presents the PSF diagrams for 0° and 20° FOVs at different spatial frequencies with an amplitude of 200 nm. Under identical error conditions, the two FOVs exhibit distinct spot shapes: an annular diffraction pattern at 0° FOV and a diffraction pattern along the y-axis at 20° FOV. Besides, the cutoff frequencies separating low, middle, and high regions for the two FOVs are similar.

When the spatial frequency exceeds 1.25 mm^{-1}, energy is transferred from the center of the focused spot to the initial diffraction rings, causing the maximum intensities of the spots to decrease to 33.3% and 34.9% of their values in the ideal model. Additionally, a broad scattering halo emerges when the spatial frequency exceeds 10 mm^{-1},

significantly reducing the energy at the spot center, with maximum intensities dropping to 0.8% and 0.5%, respectively. Compared to the ideal condition, the diameter of the scattering range is over 10 times larger. The diffraction encircled energy (Fig. 4) associated with frequency errors of 0, 1.25, 2.50, and 10.00 mm^{-1} indicates that the spot energy remains concentrated within a diameter of 50 μm when the error frequency is below 1.25 mm^{-1}. However, when the frequency increases to 10 mm^{-1}, only 50% of the energy is contained within a 100 μm diameter. These results highlight significant energy scattering loss. Therefore, for the errors on S1, the frequencies of 1.25 mm^{-1} and 10 mm^{-1} can be approximately identified as the maximum cutoff frequencies for the low and middle spatial frequency regions, respectively. The results are consistent with the literature [8, 9].

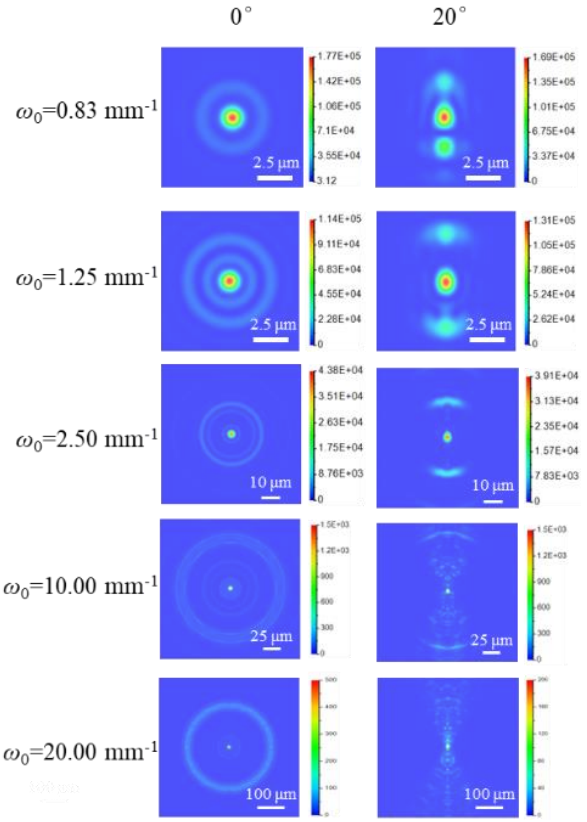

Fig. 3 Simulated field-dependent PSFs resulting from sinusoid structure errors on S1.

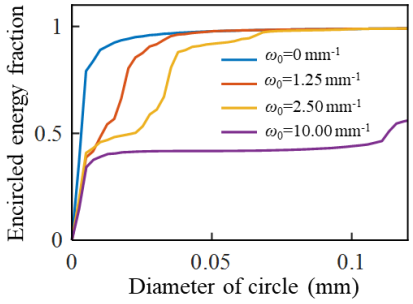

Fig. 4 Diffraction encircled energy for frequency errors of 0, 1.25, 2.50 and 10.00 mm^{-1}.

Different surfaces exhibit variations in the classification of low, mid, and high spatial frequency regions. The PSFs illustrated in Fig. 5 for the 0° FOV demonstrate the effects of various frequency errors on surfaces S3 and S5. At a spatial frequency of 1.25 mm^{-1}, energy is predominantly concentrated in the initial diffraction rings, consistent with the results for the 0° FOV shown in Fig. 3, where the S1 is the error surface. However, the maximum intensity of the central spot decreases to 8.6% and 44.0% of the ideal model for surfaces S3 and S5, respectively. Although the beam apertures for these two surfaces are comparable, which is 1.7329 mm for S3 and 1.48 mm for S5, the errors on S3 substantially reduce the energy of the central spot. Furthermore, the former diffraction spot is larger, indicating a lower cutoff frequency for the low-frequency region. There is a broad scattering halo when the error frequency reaches 10 mm^{-1} on S3, causing the maximum intensity of the central spot to drop to 0.2%. This intensity remains at 0.6% until the error frequency on S5 increases to 20 mm^{-1}, which also suggests a larger cutoff frequency for the middle-frequency region on S3 relative to S5. Compared to the results for the 0° FOV presented in Fig. 3, the cutoff frequencies for the low and middle-frequency regions are highest for S2, followed by S1, and then S5.

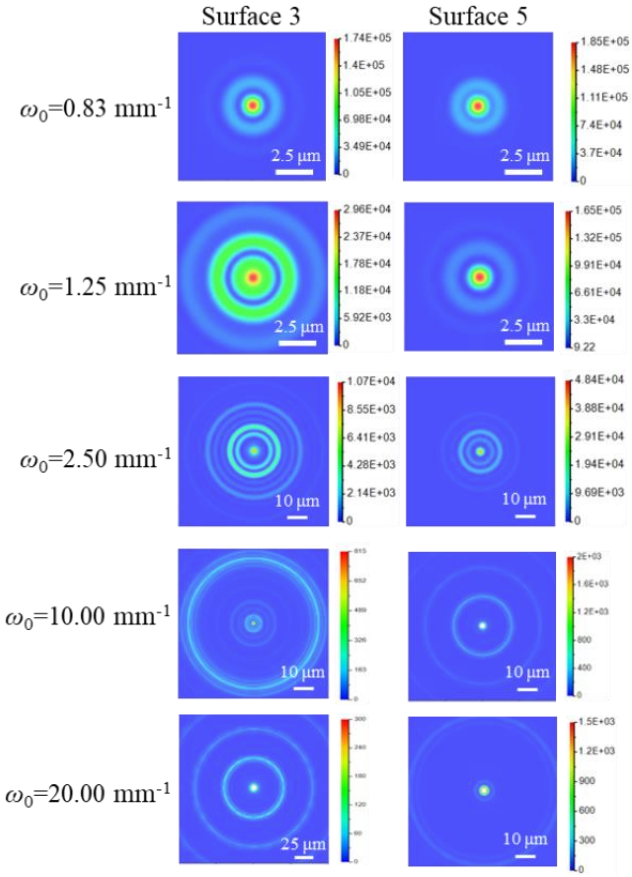

Fig. 5 PSFs of 0° FOV due to cosine structure errors on surface 3 and surface 5.

Wavelength is another critical factor influencing cutoff frequencies. The PSFs for the 0° FOV under various frequency errors at wavelengths of 656 nm and 486 nm are displayed in Fig. 5. At an error frequency of 1.25 mm^{-1} on the surface S3, the maximum intensity of the central spot decrease to 17.2% and 5.2% of the ideal model for the respective wavelengths. Notably, shorter wavelengths lead to a more significant reduction in central spot intensity caused by the error. When the error frequency exceeds 10 mm^{-1}, the maximum intensities of the

central spots further decline to 0.08% and 0.10%, indicating substantial energy scattering loss. The maximum intensities of the central spot do not vary significantly with wavelength because the central spot energy is no longer dominant. As illustrated in Fig. 6, the diffraction encircled energy reveals a large amount of energy scattered over a diameter greater than 0.1 mm. Besides, a longer wavelength results in a larger area of scattering affected by the error.

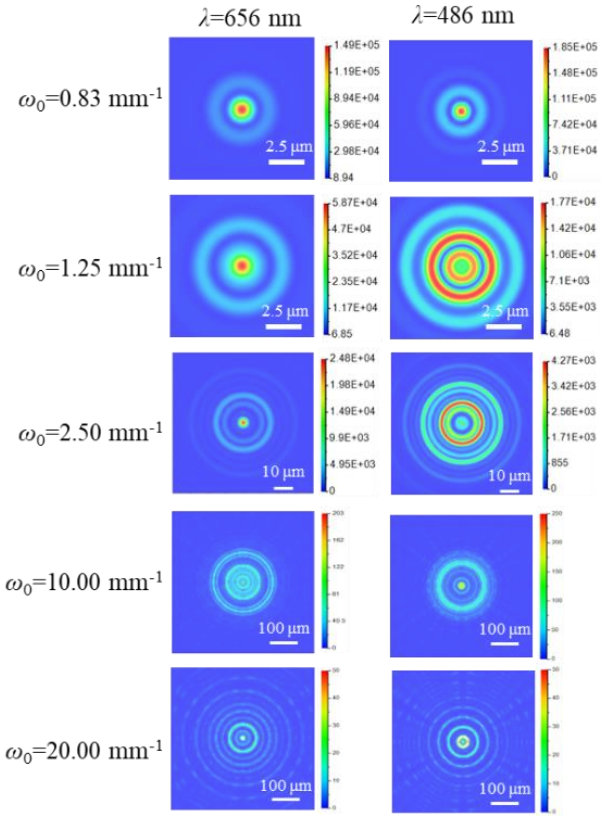

Fig. 6 PSFs of 0° FOV at 656 nm and 486 working wavelengths on the image plane, respectively.

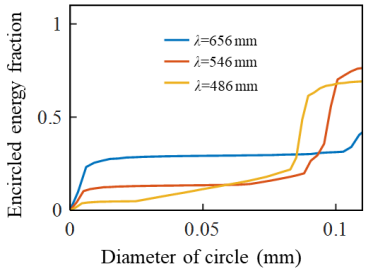

Fig. 7 Diffraction encircled energy at 656 nm, 546 nm, and 486 nm wavelength.

3. Conclusions

This paper systematically investigates the relationships between cutoff frequencies of the low, middle, and high spatial frequency regions and PSFs, focusing on variables including FOVs, surface positions, and working wavelengths. A surface error model using sinusoids is established to characterize structural errors in ultra-precision diamond turning. The main conclusions are summarized as follows:

For the designed optical system with diffraction-limited performance, the approximate maximum cutoff frequencies of 1.25 mm^{-1} and 10 mm^{-1} are identified for the low and middle spatial frequency regions on surface S1, respectively. When the surfaces are far from the stop, the effects of the surface errors on imaging performance are field-dependent.

The surface positions also affect the categorization of the low, middle, and high-frequency regions. The cutoff frequencies for the low and middle-frequency regions are highest for S2, followed by S1, and then S5.

In the low-frequency region, shorter wavelengths result in a greater reduction in the intensity of the central spot due to errors. Additionally, in the high frequency region, longer wavelengths cause a larger area of scattering affected by the error.

ACKNOWLEDGEMENT

This work was supported by the National Natural Science Foundation of China (No. 52035009).

REFERENCES

1. F. Fang, "Atomic and close-to-atomic scale manufacturing: perspectives and measures," International Journal of Extreme Manufacturing **2**, 030201 (2020).
2. F. Fang, "On the three paradigms of manufacturing advancement," Nanomanufacturing and Metrology **6**, 35 (2023).
3. J. Harvey and A. Thompson, "Scattering effects from residual optical fabrication errors," Proc. SPIE **2576**, 155-174 (1995).
4. J. Harvey, "Integrating optical fabrication and metrology into the optical design process," Applied optics **54**(9), 2224-2233 (2015)
5. D. M. Aikens, et al., "Specification and control of mid-spatial frequency wavefront errors in optical systems," Optical Fabrication and Testing, OTuA1.
6. J. M. Tamkin and T. D. Milster, "Effects of structured mid-spatial frequency surface errors on image performance," Applied Optics **49**, 6522-6536 (2010).
7. Z. Hosseinimakarem, "Mid-spatial frequency characterization and specification for freeform surfaces using Zernike polynomials," (The University of North Carolina at Charlotte, 2017).
8. J. M. Tamkin, et al., "Theory of point-spread function artifacts due to structured mid-spatial frequency surface errors," Applied Optics **49**, 4814-4824 (2010).
9. J. M. Tamkin Sr, *A study of image artifacts caused by structured mid-spatial frequency fabrication errors on optical surfaces* (The University of Arizona, 2010).